Epidemiol. Infect. (2016), **144**, 333–345. © Cambridge University Press 2015
doi:10.1017/S0950268815001739

Assessing coughing-induced influenza droplet transmission and implications for infection risk control

Y.-H. CHENG[1], C.-H. WANG[1], S.-H. YOU[2], N.-H. HSIEH[3], W.-Y. CHEN[4], C.-P. CHIO[5] AND C.-M. LIAO[1]*

[1] *Department of Bioenvironmental Systems Engineering, National Taiwan University, Taipei, Taiwan, ROC*
[2] *National Environmental Health Research Center, National Health Research Institute, Miaoli County, Taiwan, ROC*
[3] *Institute of Labor, Occupational Safety and Health, Ministry of Labor, New Taipei City, Taiwan, ROC*
[4] *Department of Biomedical Science and Environmental Biology, Kaohsiung Medical University, Kaohsiung, Taiwan, ROC*
[5] *Institute of Occupational Medicine and Industrial Hygiene, College of Public Health, National Taiwan University, Taiwan, ROC*

Received 8 February 2015; Final revision 3 June 2015;
first published online 27 July 2015

SUMMARY

Indoor transmission of respiratory droplets bearing influenza within humans poses high risks to respiratory function deterioration and death. Therefore, we aimed to develop a framework for quantifying the influenza infection risk based on the relationships between inhaled/exhaled respiratory droplets and airborne transmission dynamics in a ventilated airspace. An experiment was conducted to measure the size distribution of influenza-containing droplets produced by coughing for a better understanding of potential influenza spread. Here we integrated influenza population transmission dynamics, a human respiratory tract model, and a control measure approach to examine the indoor environment–virus–host interactions. A probabilistic risk model was implemented to assess size-specific infection risk for potentially transmissible influenza droplets indoors. Our results found that there was a 50% probability of the basic reproduction number (R_0) exceeding 1 for small-size influenza droplets of 0·3–0·4 μm, implicating a potentially high indoor infection risk to humans. However, a combination of public health interventions with enhanced ventilation could substantially contain indoor influenza infection. Moreover, the present dynamic simulation and control measure assessment provide insights into why indoor transmissible influenza droplet-induced infection is occurring not only in upper lung regions but also in the lower respiratory tract, not normally considered at infection risk.

Key words: Airborne transmission, indoor air quality, influenza, respiratory droplet, risk assessment, ventilation.

INTRODUCTION

Airborne virus droplets are a major cause of human respiratory diseases [1]. Humans spend nearly 90% of their lives indoors [1]. A number of studies have evidenced the factors influencing aerosol transmission of infection in indoor environments [1–4]. Recently, transmission and control of exhaled infectious diseases indoors have received substantial attentions [5, 6]. Airborne infectious pathogens of severe respiratory diseases originate from various sources in indoor environments where humans are found to be the major source [7, 8].

* Author for correspondence: Dr C.-M. Liao, Department of Bioenvironmental Systems Engineering, National Taiwan University, Taipei, 10617, Taiwan, ROC.
(Email: cmliao@ntu.edu.tw)

Influenza is a major disease of humans and claims tens of thousands of lives worldwide annually [6]. Therefore, to clearly examine the risk of human infection indoors posed by infectious influenza virus was a valuable issue focusing on the association between human pulmonary mechanism, different human activities, and inhaled/exhaled virus droplet concentrations. Influenza infection has been documented by experimental human exposure [9].

It has been suggested that the upper respiratory tract (nose, mouth, throat) is the primary location of droplet formation [10, 11]. Humans and their activities are linked to a number of processes resulting in the introduction of droplets with infectious content into indoor air. Duguid [10] indicated that respiratory droplets could be described by a lognormal (LN) distribution with a geometric mean (GM) of 14 μm and a geometric standard deviation (GSD) of 2·6 for cough and a GM of 8·1 μm and a GSD of 2·3 for sneeze. Loudon & Roberts [11] reported that exhaled droplets had a GM of 12 μm with a GSD of 8·4 for cough.

Fabian *et al.* [12] recently indicated that the exhaled influenza virus RNA generation rate was in the range of <3·2–20 influenza virus RNA droplets min^{-1} and up to 87% of droplets exhaled were <1 μm in diameter. They suggested that influenza virus may be contained in tidal breathing-mediated fine droplets that may play a crucial role in the spread of influenza. Lindsley *et al*. [3] indicated that coughing by influenza patients emitted aerosol droplets containing influenza virus within the respirable size range (65% of influenza RNA was contained in droplets of <4 μm aerodynamic diameter). Altogether, airborne transmission plays an important role in influenza transmission.

Because transmission via respiratory droplets and aerosols is the main route for efficient transmission between humans indoors, it is important to gain insights into airborne transmission for inhaled/exhaled influenza droplets. Moreover, human infection associated with recent emergence of influenza outbreaks highlights the need for increased understanding of the determinants for efficient indoor airborne influenza transmission in humans. In this study, we focused on studying the mechanisms of virus infection on the human respiratory tract and assessing human activities that may affect the inhaled/exhaled virus droplet concentrations from coughing by infected individuals using environmental and epidemiological influenza dynamics.

This study aimed to develop a framework for quantifying the indoor influenza infection risk based on the relationships between inhaled/exhaled respiratory droplet dynamics and population transmission dynamics. Here we treated built environment as an ecosystem to better understand the impacts of building environment–virus–host interactions on human public health posed by influenza infection. The impacts of potential control measures on environmental and epidemiological dynamics of influenza in an office were also implicated.

MATERIALS AND METHODS

Experiment

To characterize the influenza droplets indoors, an experiment of coughing-driven respiratory activities was conducted. A small airtight box measuring 36·6 cm × 50·8 cm × 30·5 cm inside was used to investigate droplet characteristics [11, 13]. The box, made of Plexiglas with an entry hole of 100 mm in diameter at the front wall for respiratory droplet expulsion from a participant's mouth, was housed in a clean meeting room with volume of nearly 45 m^3 (dimensions: 5·61 m × 3·33 m × 2·43 m). There were four non-smoking influenza-like-illness participants aged between 20 and 30 years. Before the experiment, written informed consent was required and all participants were asked to give their assent.

After turning on the monitor and waiting for 15 min, the participant was asked to enter into the clean meeting room, sit on the chair before the box and wait for another 15 min. The participant then carried out the expiratory coughing activity 20 times in 1 min [13]. After the expiratory activity was completed, the participant waited for 15 min and left. The dust monitor was then turned off after another 15 min. The total monitoring time for each participant was 61 min. Exhaled droplets in the box were measured by a dust monitor (Grimm 1.108, Germany) with 15 sampling channels (size 0·3–20 μm) to estimate the real-time droplet size characteristics of emitted, suspended or settled particles. In addition, sampling was conducted with a volume flow rate of 1·2 l min^{-1} at an interval of 6 s to measure every two coughs. Before and after each experiment, the sampling box was cleaned three times with 75% alcohol and then four times with distilled water. Particle number measurement from each coughing experiment was performed in the airtight box at a temperature and relative humidity (RH) range of 25–26 °C and 90–91%, respectively. Particle concentration inside the box could then be estimated by subtracting the

concentration in the box from the background concentration in environment measured by Grimm 1.109 (Germany).

Disease population transmission model

The environmental and epidemiological dynamics of influenza can be characterized by a typical susceptible-infected-recovered (*SIR*) epidemic model incorporating a disease transmission process occurring in the environment (E). Here an environmental infection transmission system (EITS) model was used to describe the disease population transmission (see Supplementary Fig. S1) [2]. Note that this study assumed all individuals were susceptible and there were no close contact interactions between infectious and susceptible individuals. The possible transmission route may only be aerosol transmission. In brief, disease transmission is triggered when the pathogens are released by an infected individual I and deposited into the environment E at a rate α (pathogens person^{-1} day^{-1}). All populations S, I, and R have an equal chance to pick up pathogens from E at a rate ρ (person^{-1} day^{-1}). There is a probability π (referred to as infectivity) of S becoming I per pathogen E picked up (person pathogen^{-1}). I could turn into R by a rate of recovery γ (day^{-1}). On the other hand, pathogens could be eliminated from E by decontamination or dying off with an environmental removal rate μ (day^{-1}). Thus, the dynamic equations of an EITS model can be expressed as (Fig. S1),

$$\frac{dS}{dt} = -S\rho\pi E, \tag{1}$$

$$\frac{dI}{dt} = S\rho\pi E - \gamma I, \tag{2}$$

$$\frac{dR}{dt} = \gamma I, \tag{3}$$

$$\frac{dE}{dt} = \alpha I - \left[\rho(S + I + R) + \mu\right]E, \tag{4}$$

$$N(t) = S(t) + I(t) + R(t). \tag{5}$$

A crucial concept in infection control is the basic reproduction number R_0, defined as the average number of secondary successfully infected cases caused by a typical primary infected case in an entirely susceptible population [14]. R_0 can be used to characterize the transmissibility of one disease and its likely impact on possible interventions. Based on the EITS model, R_0 has the form [2]:

$$R_0 = \frac{\alpha\rho N\pi}{\gamma(\rho N + \mu)}. \tag{6}$$

Deposition model

In an indoor environment, we usually take into account settling, deposition, inactivation, and ventilation as the virus droplet removal mechanisms in that settling and deposition rates are size-dependent [15]. In general, inactivation rate is associated with RH [16]. Therefore, the time-dependent droplet concentrations indoors can be described as [1],

$$C(t) = C_0 \exp[-(s + d + k + v)t], \tag{7}$$

where C_0 is the initial droplet concentration (m^{-3}), $C(t)$ is the environmental droplet concentration at time t(m^{-3}), and s, d, k, and v represent size range-specific settling and deposition, RH-specific inactivation, and ventilation rate (day^{-1}), respectively.

On the other hand, deposition of influenza droplets in respiratory tracts could be assessed by the human respiratory tract (HRT) model (see Supplementary material). ICRP [17] suggested that HRT can be divided into three major regions: (i) the head airways region including two compartments of nose (ET1) and mouth, pharynx, and larynx (ET2); (ii) the tracheobronchial region including two compartments of bronchial (BB) comprising trachea and bronchi and bronchiolar (bb) comprising bronchioles and terminal bronchioles; and (iii) the alveolar-interstitial (AI) region comprising the airway from respiratory bronchioles through alveolar ducts and sacs to interstitial connective tissues.

Based on the principle of mass balance, the size-dependent dynamic equations for each regional compartment can be constructed and represented by a linear state-space model [eqn (S1) in the Supplementary material]. Briefly, four main respiratory deposition mechanisms and their related constants in the HRT model could be characterized by turbulent diffusive deposition rate λ_d (s^{-1}), gravitational settling rate λ_s (s^{-1}), inertial impaction rate λ_{im} (s^{-1}), and interception deposition efficiency ε (%) (see Supplementary Figs S2, S3, Table S1). Lung physiological parameters together with deposition parameters used to estimate deposition rate coefficients and the estimated results are given in Supplementary Tables S2–S4, respectively.

Probabilistic risk model

To understand the linkages between the magnitude of internal influenza virus dose in the respiratory tract and the infection probability as well as disease transmissibility, two dose-response relationships were explored and constructed: (**i**) the association between viral titres (C_v) measured by 50% tissue culture infective dose per millilitre ($TCID_{50}$ ml^{-1}) and the infection fraction $P(I)$: $P(P(I)|C_v)$ [18] and (ii) the relationship between R_0 and $P(I)$: $P(P(I)|R_0)$ [19, 20]. Yang & Marr [1] reported that nearly 1000 influenza virus-containing droplets can contribute to 1 $TCID_{50}$ ml^{-1}. Based on this relationship, deposited droplet concentrations in each HRT region can be converted into viral titres.

The disease transmission risk probability ($P(R_{R_0}(C_v))$) can be estimated by multiplying the probability density function (pdf) of size-specific viral titres in HRT regions ($P(C_v)$) with the conditional probability of R_0 at the given level of viral titres ($P(R_0|C_v)$) constructed by coupling two dose-response profiles of $P(P(I)|C_v)$ and $P(P(I)|R_0)$,

$$P(R_{R_0(C_v)}) = P(C_v) \times P(R_0|C_v). \tag{8}$$

The statistical models were fitted to study data to select the best-fitted models based on the least squares criterion from a set of generalized linear and nonlinear autoregression models provided by TableCurve 2D packages (AISN Software Inc., USA). A value of $P < 0{\cdot}05$ was judged significant. The uncertainty and its impact on the expected risk estimate were quantified by a Monte Carlo (MC) simulation technique that was carried out with 10 000 iterations to assure the stability of those pdfs and generate 2·5 and 97·5 percentiles as the 95% confidence interval (CI) for all fitted models. Crystal Ball® software version 2000.2 (Decisioneering Inc., USA) was employed to implement the MC simulation.

Control measure model

Asymptomatic infectious proportion (θ) can be used to estimate the proportion of transmission occurring prior to onset of symptoms [21]. Thus the potential of public health control measures based on symptomatic population can be estimated. By definition, θ can be calculated as [21],

$$\theta = \frac{\tau_I - \tau_L}{\tau_V}, \tag{9}$$

where τ_I is the incubation period estimated from occurrence of infection to appearance of symptoms, τ_L is the latent period estimated from occurrence of infection to infectious state beginning, and $\tau_V$is the mean duration of viral shedding.

Fraser *et al.* [21] developed a two-efficacy-based control measure model by considering two key epidemiological determinants R_0 and θ as well as the control efficacy ε. In this study, we used three common indoor control measures of ventilation filter [22], hand washing [23], and active carbon mask [24] with efficacies ε_F, ε_H, ε_M, respectively, weighed in the R_0–θ control model [25],

$$R_0\left\{\begin{array}{l}(1-\varepsilon_F)(1-\varepsilon_M)(1-\varepsilon_H)+[\varepsilon_F(1-\varepsilon_M)(1-\varepsilon_H)\\ +\varepsilon_M(1-\varepsilon_F)(1-\varepsilon_H)+\varepsilon_H(1-\varepsilon_F)(1-\varepsilon_M)]\theta\\ +[\varepsilon_F\varepsilon_M(1-\varepsilon_H)+\varepsilon_F\varepsilon_H(1-\varepsilon_M)\\ +\varepsilon_M\varepsilon_H(1-\varepsilon_F)]\left(\frac{\theta}{2-\theta}\right)+(\varepsilon_F\varepsilon_M\varepsilon_H)\left(\frac{\theta}{3-2\theta}\right)=1.\end{array}\right\} \tag{10}$$

Theoretically, eqn (10) is a control curve shown in the R_0–θ coordinate system. Generally, above the critical control curve, control measure would be additionally required to control the disease spread [21].

RESULTS

Coughing-induced virus droplet characteristics

Figure 1*a* shows that the experimental droplet nuclei size-specific number of concentrations for coughing can be well described by a LN model with GM 0·33 μm and GSD 1·23 [LN(0·33 μm, 1·23), $r^2 =$ 0·99, $P < 0{\cdot}001$], revealing that no significant skew of concentration distribution existed. The results indicated that droplet number concentrations were $5{\cdot}82 \times 10^8$, $1{\cdot}94 \times 10^8$, $1{\cdot}98 \times 10^7$, and $7{\cdot}63 \times 10^5$ m^{-3} μm^{-1} corresponding to sizes ranging from 0·3–0·4, 0·4–0·5, 0·5–1, and 1–5 μm, respectively (Fig. 1*a*).

We also found that the deposition rate for 0·3–0·4 μm droplet size was highest in all size ranges at 1 m horizontal distance and decreased with increases in time and horizontal distance (Fig. 1*b*), while similar relationships could be observed at for 0·4–0·5, 0·5–1, and 1–5 μm (Fig. 1*c*–*e*). The relationship between RH and inactivation rate can be constructed based on the published data ($y = -0.29 + 0.01x$, $r^2 = 0{\cdot}82$, $P < 0{\cdot}001$), indicating that on average the inactivation rates ranged from 0·27 to 0·71 h^{-1} at a common RH range of 40–70% in an indoor environment (Fig. 1*f*).

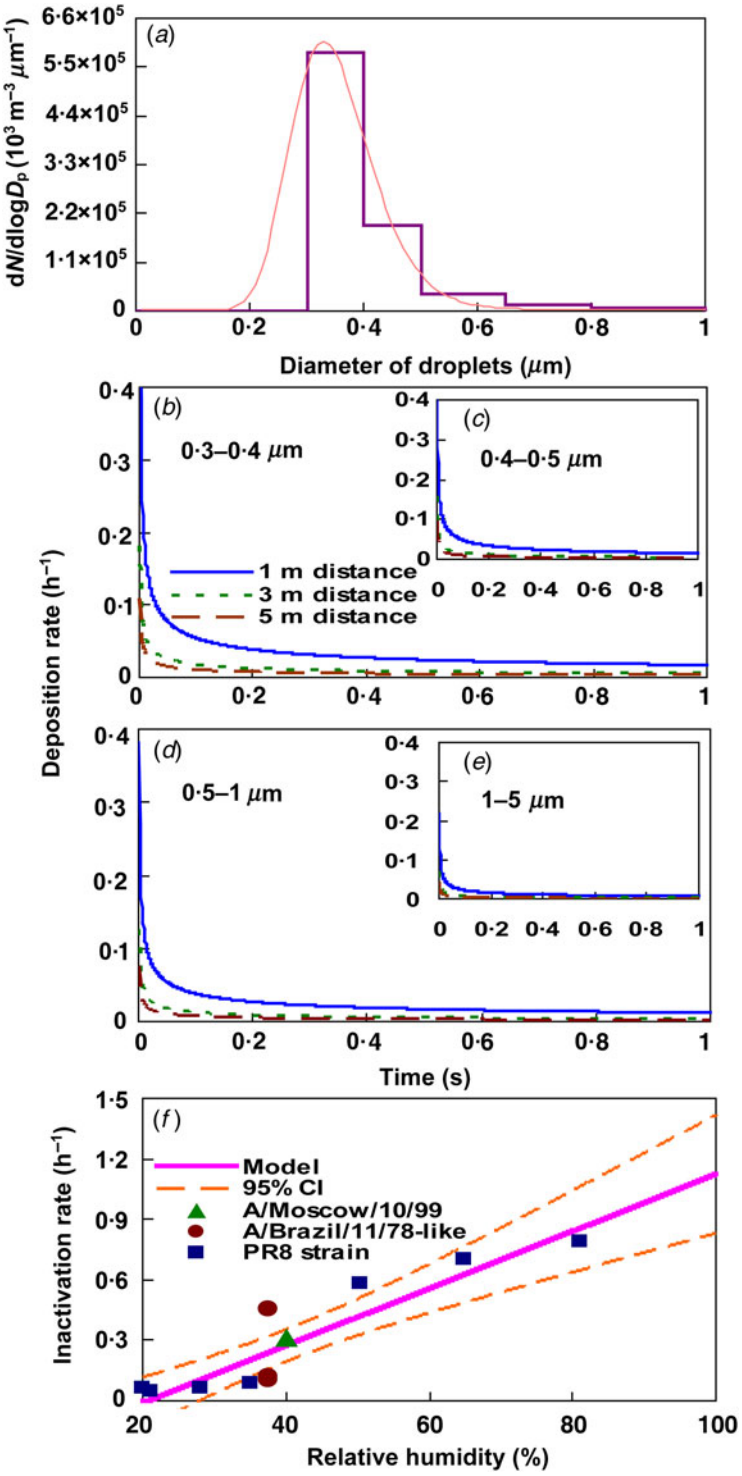

Fig. 1. (*a*) Droplet number concentrations for different size ranges. (*b–e*) Time-dependent deposition rates characterized by different horizontal distances for four ranges. (*f*) Relative humidity inactivation rate relationship.

Population transmission and incidence

Our results indicated that the environmental droplet number concentrations sized 0·3–0·4 μm decreased rapidly over time followed by concentrations of 0·4–0·5, 0·5–1, and 1–5 μm (Fig. 2*a*, *b*). As time reached 1 h, the environmental droplet number concentration fell to 0 where averaged droplet concentrations were $5{\cdot}68 \times 10^7$, $1{\cdot}92 \times 10^7$, $1{\cdot}98 \times 10^6$, and $6{\cdot}67 \times 10^4$ m^{-3}

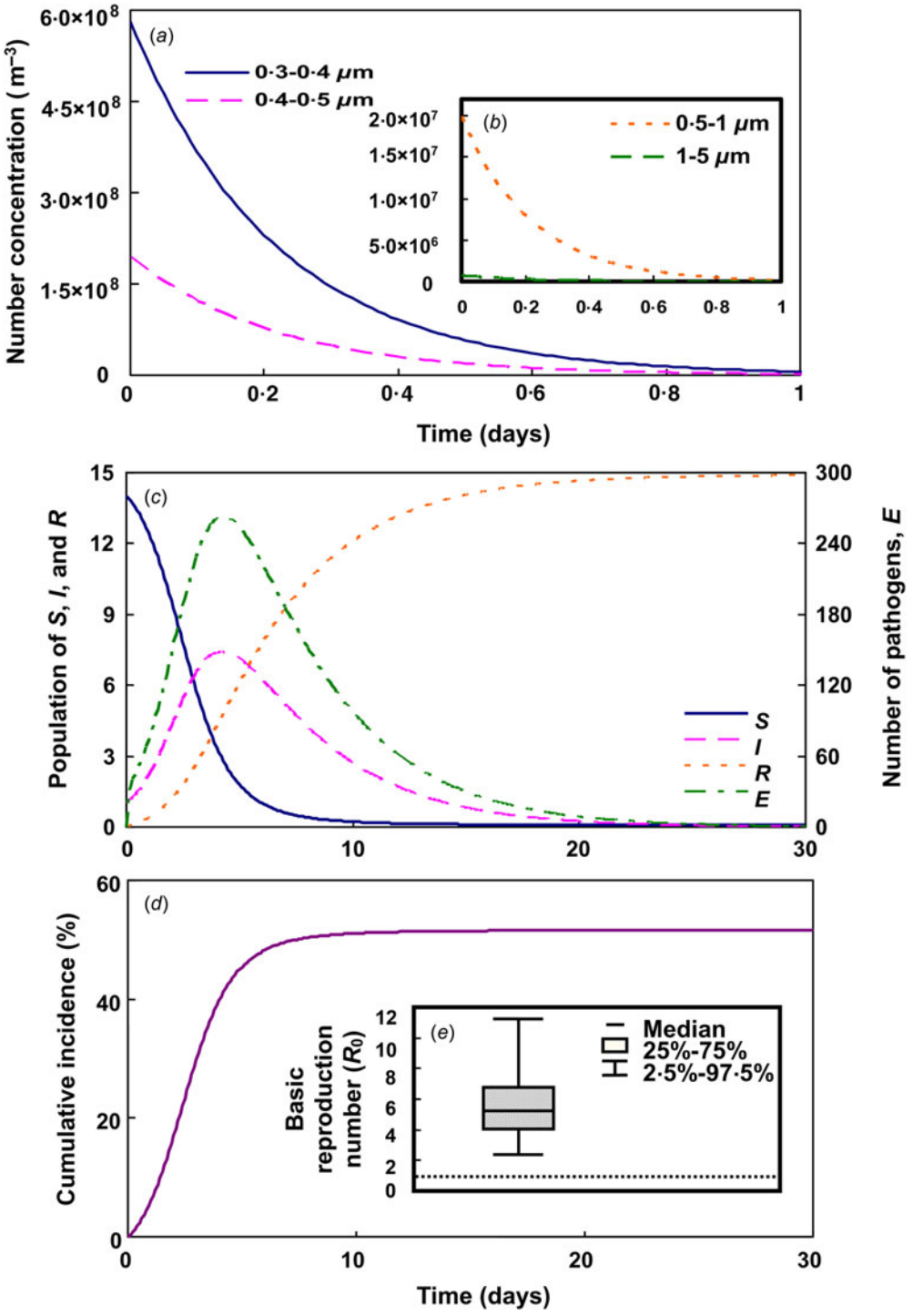

Fig. 2. Environmental droplet number concentrations decrease with time and size in settling and deposition rates for (*a*) 0·3–0·4 and 0·4–0·5 and (*b*) 0·5–1 and 1–5 μm range from 0·005–0·476 and 0·05–0·14 h^{-1}, respectively, with inactivation rate of 0·49 h^{-1} and ventilation rate of 4 h^{-1}. (*c*) Transmission dynamics of *S, I, R*, and *E* in the EITS-based model. (*d*) Time-dependent cumulative incidence of influenza infection. (*e*) Box-whisker plot of the basic reproduction number (R_0) estimates.

at time interval 0–0·5 h (the time that $C(t)$ reached its half maximum droplet number concentration) for 0·3–0·4, 0·4–0·5, 0·5–1, and 1–5 μm, respectively.

The results of the EITS model parameterization are listed in Supplementary Table S5. The disease transmission dynamics were simulated within 30 days with initial

conditions of 14, 1, 0 (numbers) and 0 (pathogens), respectively, for *S, I, R*, and *E* in an office setting. On days 4·2 and 4·3, the expected infected numbers and the live pathogens indoors reached their peak values of 7 and 263, respectively, whereas susceptibles were reduced to 1 and people recovered to health on days 6 and 30, respectively (Fig. 2*c*). On the other hand, the transient cumulative incidence reached 50% at day 7·4 and then approached steady state (Fig. 2*d*). The estimated R_0 was 5·22 (95% CI 2·40–11·26), indicating that in an indoor environmental setting like an office, influenza virus spreads severely and control measures are essential for prevention of further disease outbreaks (Fig. 2*e*).

To investigate parameters contributing to the EITS model, a sensitivity analysis was performed. Sensitivity analysis indicated that the pick-up rate (ρ) was the most significant influence factor (68% in variance explained) followed by pathogen deposition rate (α) (15%), elimination rate (μ) (−11%), and recovery rate (γ) (−6%).

Concentration and deposition in HRT

We showed that all the size range-specific droplet concentrations of each HRT region were likely to reach equilibrium in the first 20 s, thus, the equilibrium droplet concentrations dominate the deposition dynamics (Fig. 3*a–d*). Overall, the deposited droplet number concentration of 0·3–0·4 μm would count highest in all HRT regions, giving a total concentration of $2{\cdot}34 \times 10^7$ m^{-3} followed by 0·4–0·5, 0·5–1, and 1–5 μm with total concentrations of $7{\cdot}24 \times 10^6$, $5{\cdot}42 \times 10^5$ and $1{\cdot}48 \times 10^4$ m^{-3}, respectively (Fig. 3*a–d*). On the other hand, the total number concentrations deposited in ET1, BB, bb, and AI regions were $9{\cdot}69 \times 10^4$, $3{\cdot}57 \times 10^5$, $9{\cdot}74 \times 10^6$, and $2{\cdot}10 \times 10^7$ m^{-3}, respectively (Fig. 3*a–d*).

We found that the larger droplet size inhaled was more likely to accumulate in ET1, BB, and bb regions (Fig. 3*e*). Noticeably, in the AI region, as inhaled droplet size increased, the deposition fraction rarely increased for sizes 0·3–0·4, 0·4–0·5, and 0·5–1 μm with the value ranging from 0·157 to 0·169. However, it reduced substantially to 0·047 for 1–5 μm (Fig. 3*e*).

Size-specific infection risk estimates

Our results indicate that the relationship between R_0 and infection fraction ($P(I)$) is well described by an exponential function of $y = 1 - \exp(1.24 - 1.30x)$ ($r^2 = 0{\cdot}94$, $P < 0{\cdot}001$) (Fig. 4*a*). The results show that R_0 estimates of 1·5 and 2 would lead to infection fractions of 0·4 and 0·67, respectively, whereas $R_0 \geqslant 4$ resulted in an infection fraction of nearly 1. On the other hand, the relationship between viral titre (C_v) and $P(I)$ was best fitted with a power law function [$y = x^{6.75}/(5.68^{6.75} + x^{6.75})$, $r^2 = 0{\cdot}90$, $P < 0{\cdot}001$] where viral spread could lead to infection only when the viral titre is >1000 TCID$_{50}$ ml^{-1} (Fig. 4*b*). Finally, the viral titre−R_0 profile can be optimally obtained and described by a nonlinear equation of $y = 0.37 + 0.04x^2$ ($r^2 = 0{\cdot}99$, $P < 0{\cdot}001$) (Fig. 4*c*).

Our results show that the viral titre distributions could be well described by a LN model with a median of 4·03 (95% CI 3·68–4·40), 3·53 (95% CI 3·25–3·82), 2·41 (95% CI 2·34–2·49), and 0·77 (95% CI 0·67–0·88) log$_{10}$ TCID$_{50}$ ml^{-1} for size ranges 0·3–0·4, 0·4–0·5, 0·5–1, and 1–5 μm, respectively (Fig. 5*a*). We found that there was no probability of R_0 exceeding 1 for sizes 0·4–0·5, 0·5–1, and 1–5 μm (Fig. 5*b*). However, there were at least 50% and 10% probabilities of R_0 estimates falling between 0·87–1·03 and 0·94–1·10, respectively, for the 0·3–0·4 μm droplet size range (Fig. 5*b*).

Control measure applications

Based on an estimated R_0 of 5·22 (95% CI 2·4–11·26) (Fig. 2*e*) and θ of 0·29 (95% CI 0·15–0·55) (Fig. 6*a*), an indoor R_0–θ control curve for influenza infections can then be constructed (Fig. 6*b*). To achieve optimal control of influenza virus transmission, maximum control efficacies of control strategies involving ventilation filter (ε_F = 47–87%), active carbon mask (ε_M = 20–81%), and hand washing (ε_H = 36–57%) were taken into account. Here we considered three forward-additional control measure schemes designated as C1 (ε_F), C2 ($\varepsilon_F + \varepsilon_H$), and C3 ($\varepsilon_F + \varepsilon_H + \varepsilon_M$) (Fig. 6*b*).

Our results indicated that even though all interventions were implemented, the uncontrollable ratio is still 67% high (Fig. 6*b*). To prevent further influenza outbreak, vaccine is considered with 60–80% coverage [26]. We calculated vaccine-based R_0 ($R_{0,V}$) as $R_{0,V} = R_0(1 - V)$ where V is the vaccine coverage. Taking 60% vaccine coverage into account, 42–86% effective control efficiencies were obtained, whereas 70% and 80% vaccine coverage could give controllable ratios of 64–97% and 91–100%, respectively (Fig. 6*b*). In comparison with the control measures without vaccine, we showed that 60%, 70%, and 80% vaccine coverage could, respectively, enhance the disease containment up to 79%, 96%, and 100%, revealing excellent control efficacy by using vaccine.

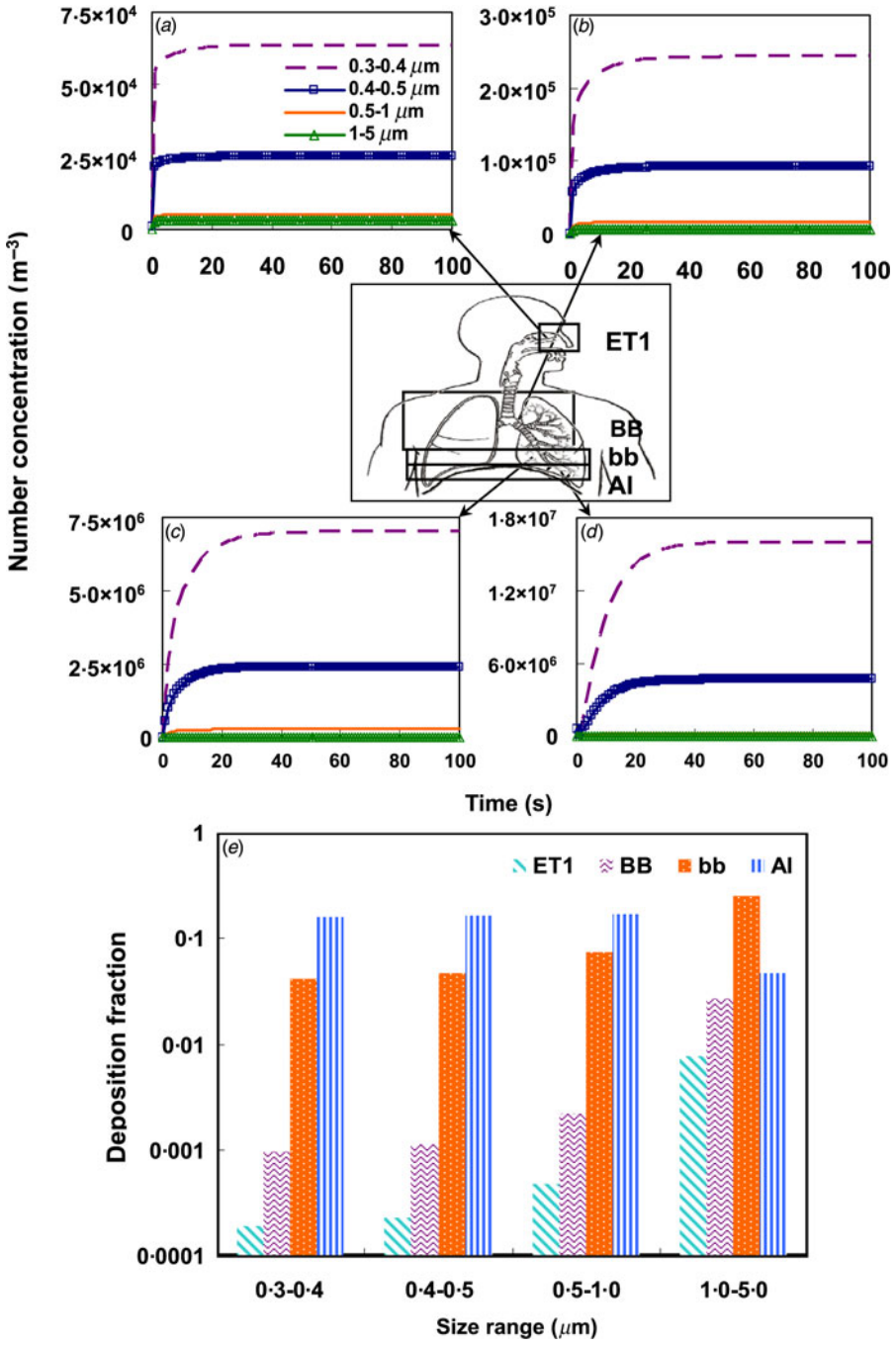

Fig. 3. Deposited droplet number concentrations for ranges 0·3–0·4, 0·4–0·5, 0·5–1, and 1–5 μm in (*a*) ET1, (*b*) BB, (*c*) bb, and (*d*) AI regions, respectively. (*e*) Human respiratory tract region-specific deposition fractions for 0·3–0·4, 0·4–0·5, 0·5–1, and 1–5 μm, respectively.

DISCUSSION

Droplet behaviour change

Our study shows that gravitational settling can remove up to 80% of droplets emitted from a cough within 10 min. Yang & Marr [1] evidenced that as droplet size increased, the settling rate increased. Our results found that the settling rate was 0·48 h^{-1} for size 0·5–1 μm much higher than that of 0·3–0·4 μm for 0·005 h^{-1}. These magnitudes of estimates were consistent with Yang & Marr [1].

Zhao *et al.* [27] indicated that aerosol droplets deposited on environmental surfaces could cause contamination and lead to further hazard. Our results

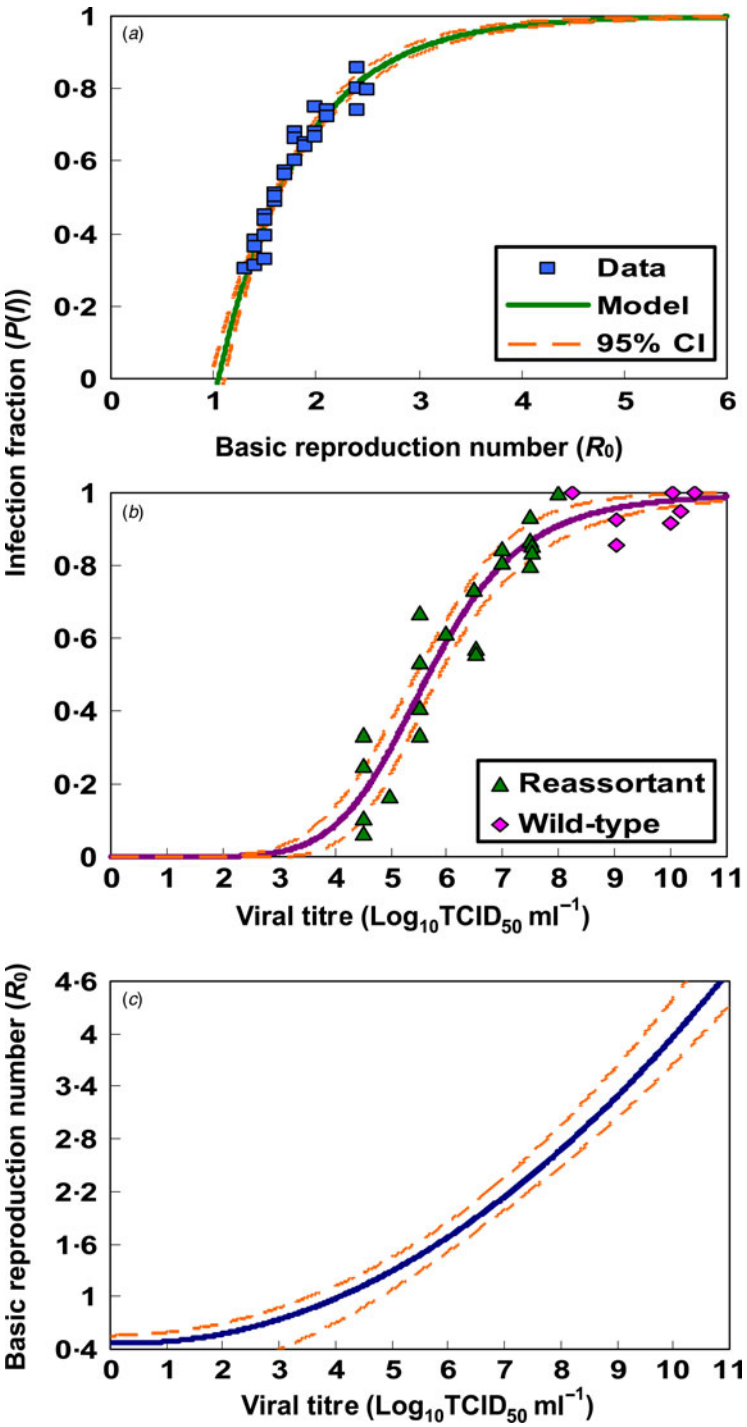

Fig. 4. Dose-response relationships between (*a*) R_0 and infection fraction and (*b*) viral titre and infection fraction. (*c*) Viral titre−R_0 relationship built by coupling (*a*) and (*b*).

indicated that removal efficiency caused by deposition was more important than settling for particle size <1 μm. Therefore, this study focused more on the deposition removal mechanism. Yang & Marr [1] indicated that the removal efficiency by inactivation was relatively low, yet it was important when removal by settling and ventilation were both insignificant. Our result is in agreement with previous studies [6, 16, 28], suggesting that inactivation rate of influenza A viruses increases with increasing RH.

RH, temperature, and ventilation are the leading factors affecting influenza infection in an indoor

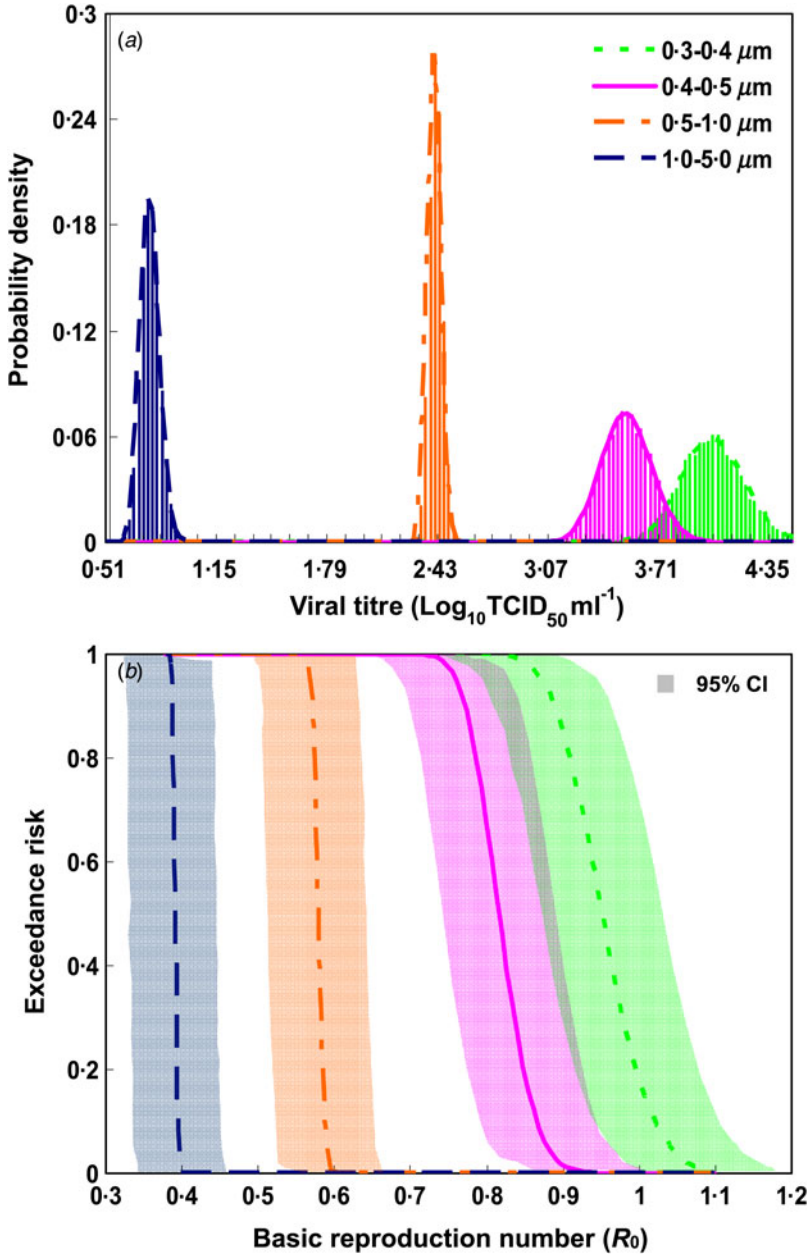

Fig. 5. (*a*) Lognormal distributions of viral titre ($TCID_{50}$ ml^{-1}) in human respiratory tract (HRT) regions for 0·3–0·4, 0·4–0·5, 0·5–1, and 1–5 μm, respectively. (*b*) Probabilistic risk profiles of R_0 given influenza virus-bearing droplets inhaled and deposited in HRT regions for 1–5, 0·5–1, 0·4–0·5, and 0·3–0·4 μm, respectively.

environment [1, 29, 30]. RH also influences both the evaporation rate and the particle equilibrium sizes [1, 5, 31]. When influenza virus-bearing droplets were exhaled from the respiratory tract, they evaporated and shrank rapidly as long as they encountered the unsaturated ambient atmosphere and RH. However, different subjects, respiratory activities, experimental conditions, and sampling techniques may cause differences in droplet size measurement. Therefore, droplet size was the key determinant in pathogen carriage, aerosolizing, and transmission [1, 5]. Human respiratory activities including breathing, talking, coughing, and sneezing; however, we chose coughing in our study since 80% of patients with influenza infection manifest symptoms as coughing [32].

Impact of host on dynamics of influenza droplets

Our study evidenced that the distributions of airspace volume, ventilation rate, and people in ventilated

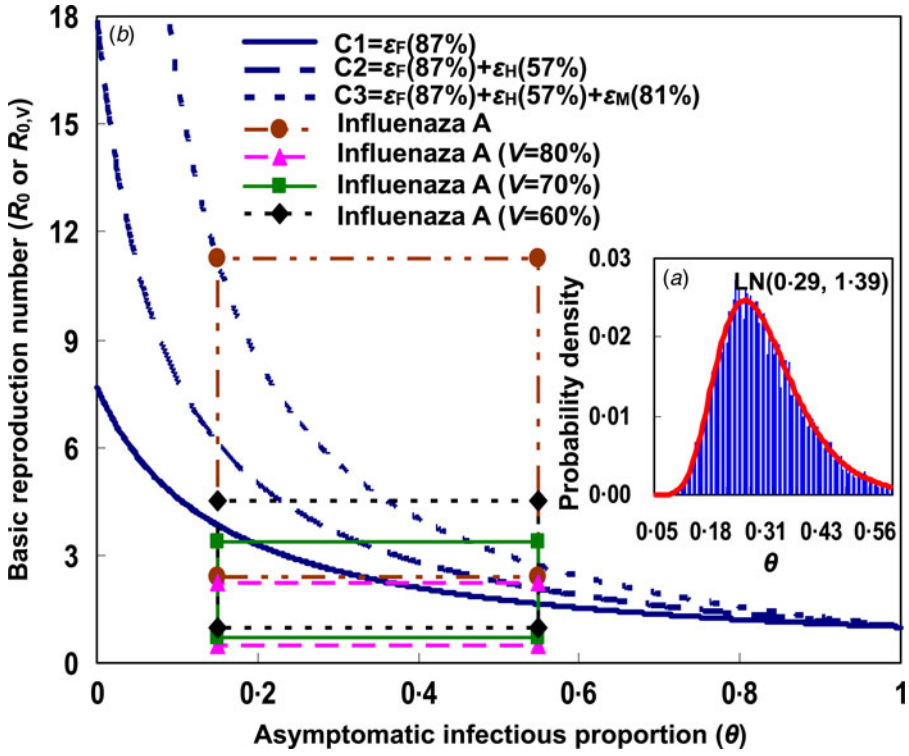

Fig. 6. (*a*) Probability distribution profile of asymptomatic infectious proportion (θ). (*b*) R_0–θ critical control curves constructed by taking into account the potential intervention combinations of ventilation filter (ε_F), hand washing (ε_H), and active carbon mask (ε_M) without vaccine coverage and with 60%, 70%, and 80% coverage.

airspaces play crucial roles in affecting influenza transmission dynamics indoors. Our R_0 estimates ranged from 2·4–11·26, indicating higher influenza infection risk in indoor environments, are consistent with published R_0 values ranging from 1·5 to 17·0, either estimated by applying a population transmission dynamic model and a mathematical epidemic equation [33, 34] or by fitting transmission models to time-series data [35, 36].

We also recognized that our analysed results followed the functional form in illustrating the relationship between R_0 and final epidemic size derived by Anderson & May [14] for an enclosed population setting (i.e. Infected proportion = $[1 - (1 + \ln\ R_0)/R_0)]$). Our median R_0 estimate was 5·22 and the corresponding final epidemic proportion was estimated as 0·5, which was approximate to our estimated maxima cumulative incidence of 50% (Fig. 2*d*).

Nevertheless, little is known about the extent to which virus is deposited by infected individuals into the environment and whether deposited virus has the ability to infect new hosts. Our proposed droplet-based population transmission dynamic model can be used to describe the dynamics of human interaction with pathogens in an indoor environment [2, 4, 37, 38].

Zhao *et al.* [27] indicated that aerosol droplets deposited on the human respiratory tract pose potential harmful effects. The respiratory deposition of droplets depends on particle size [38]. Larger droplets are trapped increasingly in the upper respiratory tract; however, small droplets are deposited in the lower respiratory tract and the alveolar region [4, 31]. Our results indicate that deposition fractions of 0·3–0·4 μm were $1{\cdot}90 \times 10^{-4}$, $9{\cdot}68 \times 10^{-4}$, 0·04 and 0·16 in regions ET1, BB, bb, and AI, respectively. Deposition fraction increased as droplet size increased in regions ET1, BB, and bb, yet a contrary result was found in region AI.

Killingley *et al.* [9] suggested that the infectious dose of aerosol inoculation ranged from 0·6–3 $TCID_{50}$ ml^{-1} and the infectious dose for intranasal inoculation ranged from 100–1000 $TCID_{50}$ ml^{-1}. The mean viral titre estimates of influenza droplets were nearly 10000, 3390, 300, and 5 $TCID_{50}$ ml^{-1} for 0·3–0·4, 0·4–0·5, 0·5–1, and 1–5 μm, respectively, indicating that they are likely to pose high indoor influenza infection risks, especially for small droplet sizes.

Limitations and implications

This study developed a three-efficacy control measure model to obtain an optimal influenza infection control

indoors. Our results indicate that vaccination plays a crucial role in enhancing control measures. However, we could not independently estimate influenza viral droplets and viral titre from our experiments. We selected influenza A for disease transmission, yet we could not classify the virus subtypes of A(H1N1) or A (H3N2). Therefore, we may consider different subtypes for influenza transmission in a future study. Many modelling works, including the present study, cannot verify droplet number concentrations in upper and lower respiratory tracts, as well as the volume distributions within specific size ranges. Therefore, this issue warrants further study.

Generally, the well-mixed environment assumption is used in a parsimonious model as described in our paper. However, in reality, influenza viruses are not distributed homogeneously in airborne droplets according to their particle size. Moreover, distribution of airborne infectious droplets may also vary with the spatial position and the location of virus sources. Because of the spatial position of droplets, humans are likely to be exposed to specific particle sizes. Therefore, for human exposure assessment purposes, our well-mixed assumption is not practically justified and the results should be interpreted with caution.

Sze To & Chao [39] indicated that the underlying factors that affect airborne transmission of infectious diseases were complex, including dispersion and distribution of airborne pathogens, ventilation strategy, survival of pathogen, aerosol size, respiratory deposition, heterogeneous infectivity, air turbulence, pathogen–host interactions, and control measures. Our study considered the above factors except dispersion and distribution of airborne pathogens, and heterogeneous infectivity, and those can also be included in a future study.

Our results highlight that the recently developed disease population transmission model incorporating a control-measure modelling approach can be used to assess exhaled and inhaled influenza droplets in an indoor environment. The present probabilistic risk model can also provide a practical template for assessing the droplet size-specific infection risks for potentially transmissible influenza virus-bearing respiratory droplets in indoor environments. We conclude that the present dynamic simulation and control-measure assessment provide insights into why indoor transmissible influenza droplet-induced infection is occurring not only in upper lung regions but also in lower respiratory tract regions not normally considered an infection risk.

SUPPLEMENTARY MATERIAL

For supplementary material accompanying this paper visit http://dx.doi.org/10.1017/S0950268815001739.

ACKNOWLEDGEMENTS

The authors acknowledge the financial support of the Ministry of Science and Technology, Republic of China under Grant MOST 104-2221-E-002-030-MY3.

DECLARATION OF INTEREST

None.

REFERENCES

1. **Yang W, Marr LC.** Dynamics of airborne influenza A viruses indoors and dependence on humidity. *PLoS ONE* 2011; **6**: e21481.
2. **Li S, *et al.*** Dynamics and control of infections transmitted from person to person through the environment. *American Journal of Epidemiology* 2009; **170**: 257–265.
3. **Lindsley WG, *et al.*** Measurements of airborne influenza virus in aerosol particles from human coughs. *PLoS ONE* 2010; **5**: e15100.
4. **Spicknall IH, *et al.*** Informing optimal environmental influenza interventions: how the host, agent, and environment alter dominant routes of transmission. *PLoS Computational Biology* 2010; **6**: e1000969.
5. **Xie X, *et al.*** How far droplets can move in indoor environments-revisiting the Wells evaporation-falling curve. *Indoor Air* 2007; **17**: 211–225.
6. **Jones RM.** Critical review and uncertainty analysis of factors influencing influenza transmission. *Risk Analysis* 2011; **31**: 1226–1242.
7. **Costello EK, *et al.*** Bacterial community variation in human body habitats across space and time. *Science* 2009; **326**: 1694–1697.
8. **Kembel SW, *et al.*** Architectural design influences the diversity and structure of the built environment microbiome. *ISME Journal* 2012; **6**: 1469–1479.
9. **Killingley B, *et al.*** Potential role of human challenge studies for investigation of influenza transmission. *Lancet Infectious Diseases* 2011; **11**: 879–886.
10. **Duguid JP.** The size and the duration of air-carriage of respiratory droplets and droplet-nuclei. *Journal of Hygiene* 1946; **44**: 471–479.
11. **Loudon RG, Roberts RM.** Droplet expulsion from the respiratory tract. *American Review of Respiratory Disease* 1967; **95**: 435–442.
12. **Fabian P, *et al.*** Influenza virus in human exhaled breath: an observational study. *PLoS ONE* 2008; **3**: e2691.
13. **Xie X, *et al.*** Exhaled droplets due to talking and coughing. *Journal of the Royal Society Interface* 2009; **6**: S703–S714.

14. **Anderson RM, May RM.** *Infectious Diseases of Humans: Dynamics and Control*. Oxford: Oxford University Press, 1991.
15. **Hinds WC.** *Aerosol Technology: Properties, Behavior, and Measurement of Airborne Particles*, 2nd edn. New York: Wiley, 1999.
16. **Thomas Y, *et al.*** Survival of influenza virus on banknotes. *Applied and Environmental Microbiology* 2008; **74**: 3002–3007.
17. **International Commission on Radiological Protection.** *Human Respiratory Tract Model for Radiological Protection: a Report of a Task Group of the International Commission on Radiological Protection*. ICRP Publication 24. Oxford: Pergamon, 1994.
18. **Watanabe T, *et al.*** Dose-response assessment for influenza A virus based on data sets of infection with its live attenuated reassortants. *Risk Analysis* 2012; **32**: 555–565.
19. **Halder N, Kelso JK, Milne GJ.** Analysis of the effectiveness of interventions used during the 2009 A/H1N1 influenza pandemic. *BMC Public Health* 2010; **10**: 168–181.
20. **Milne GJ, *et al.*** A small community model for the transmission of infectious diseases: comparison of school closure as an intervention in individual-based models of an influenza pandemic. *PLoS ONE* 2008; **3**: e4005.
21. **Fraser C, *et al.*** Factors that make an infectious disease outbreak controllable. *Proceedings of the National Academy of Sciences USA* 2004; **101**: 6146–6151.
22. **McDevitt JJ, MacIntosh DL, Myatt TA.** Removal of influenza viral aerosols by high efficiency electrostatic air cleaner and implications for household infection transmission. *Indoor Air* 2008; **18**: 17–22.
23. **Jefferson T, *et al.*** Physical interventions to interrupt or reduce the spread of respiratory viruses: systematic review. *British Medical Journal* 2008; **336**: 77–80.
24. **Huang SH.** Mask information. Taiwan: Institute of Occupational Safety and Health, 2004, IOSH Publications.
25. **Chen SC, Chang CF, Liao CM.** Predictive models of control strategies involved in containing indoor airborne infections. *Indoor Air* 2006; **16**: 469–481.
26. **Taiwan CDC (Taiwan Centers for Disease Control).** (http://www.cdc.gov.tw/professional/index.aspx). Accessed 30 December 2012.
27. **Zhao B, *et al.*** Comparison of indoor aerosol particle concentration and deposition in different ventilated rooms by numerical method. *Building and Environment* 2004; **39**: 1–8.
28. **Weber TP, Stilianakis NI.** Inactivation of influenza A viruses in the environment and modes of transmission: a critical review. *Journal of Infection* 2008; **57**:
29. **Tang JW.** The effect of environmental parameters on the survival of airborne infectious agents. *Journal of the Royal Society Interface* 2009; **6**: S737–S746.
30. **Tellier R.** Aerosol transmission of influenza A virus: a review of new studies. *Journal of the Royal Society Interface* 2009; **6**: S783–S790.
31. **Nicas M, Nazaroff WW, Hubbard A.** Toward understanding the risk of secondary airborne infection: emission of respirable pathogens. *Journal of Occupational and Environmental Hygiene* 2005; **2**: 143–154.
32. **Tang JW, *et al.*** Differing symptom patterns in early pandemic vs seasonal influenza infections. *Archives of Internal Medicine* 2010; **170**: 861–867.
33. **Rudnick SN, Milton DK.** Risk of indoor airborne infection transmission estimated from carbon dioxide concentration. *Indoor Air* 2003; **13**: 237–245.
34. **Vera DM, *et al.*** Assessing the impact of public health interventions on the transmission of pandemic H1N1 influenza a virus aboard a Peruvian navy ship. *Influenza and Other Respiratory Viruses* 2014; **8**: 353–359.
35. **Vynnycky E, Trindall A, Mangtani P.** Estimates of the reproduction numbers of Spanish influenza using morbidity data. *International Journal of Epidemiology* 2007; **36**: 881–889.
36. **White LF, Pagano M.** Transmissibility of the influenza virus in the 1918 pandemic. *PLoS ONE* 2008; **3**: e1498.
37. **Bani-Yaghoub M, *et al.*** Effectiveness of environmental decontamination as an infection control measure. *Epidemiology and Infection* 2012; **140**: 542–553.
38. **Stilianakis NI, Drossinos Y.** Dynamics of infectious disease transmission by inhalable respiratory droplets. *Journal of the Royal Society Interface* 2010; **7**: 1355–1366.
39. **Sze To GN, Chao CY.** Review and comparison between the Wells-Riley and dose-response approaches to risk assessment of infectious respiratory diseases. *Indoor Air* 2010; **20**: 2–16.